

Synthesis, characterization, redox behavior, DNA and protein binding and antibacterial activity studies of ruthenium(II) complexes of bidentate schiff bases

Hena Paul, Buddhadeb Sen, Tapan Kumar Mondal & Pabitra Chattopadhyay

To cite this article: Hena Paul, Buddhadeb Sen, Tapan Kumar Mondal & Pabitra Chattopadhyay (2017): Synthesis, characterization, redox behavior, DNA and protein binding and antibacterial activity studies of ruthenium(II) complexes of bidentate schiff bases, *Nucleosides, Nucleotides and Nucleic Acids*, DOI: [10.1080/15257770.2017.1332763](https://doi.org/10.1080/15257770.2017.1332763)

To link to this article: <http://dx.doi.org/10.1080/15257770.2017.1332763>



Published online: 14 Jul 2017.



Submit your article to this journal [↗](#)



Article views: 7



View related articles [↗](#)



View Crossmark data [↗](#)



Synthesis, characterization, redox behavior, DNA and protein binding and antibacterial activity studies of ruthenium(II) complexes of bidentate schiff bases

Hena Paul^a, Buddhadeb Sen^a, Tapan Kumar Mondal^b, and Pabitra Chattopadhyay^a

^aDepartment of Chemistry, Burdwan University, Golapbag, Burdwan, India; ^bDepartment of Chemistry, Jadavpur University, Jadavpur, Kolkata, India

ABSTRACT

Two new ruthenium(II) complexes of Schiff base ligands (L) derived from *cinnamaldehyde* and *ethylenediamine* formulated as $[\text{Ru}(\text{L})(\text{bpy})_2](\text{ClO}_4)_2$, where $\text{L}^1 = N,N'$ -bis(4-nitrocinnamaldehyde)ethylenediamine and $\text{L}^2 = N,N'$ -bis(2-nitrocinnamaldehyde)ethylenediamine for complex **1** and **2**, respectively, were isolated in pure form. The complexes were characterized by physicochemical and spectroscopic methods. The electrochemical behavior of the complexes showed the Ru(III)/Ru(II) couple at different potentials with *quasi*-reversible voltammograms. The interaction of the complexes with calf thymus DNA (CT-DNA) using absorption, emission spectral studies and electrochemical techniques have been used to determine the binding constant, K_b and the linear Stern–Volmer quenching constant, K_{sv} . The results indicate that the ruthenium(II) complexes interact with CT-DNA strongly in a groove binding mode. The interactions of bovine serum albumin (BSA) with the complexes were also investigated with the help of absorption and fluorescence spectroscopy tools. Absorption spectroscopy proved the formation of a ground state BSA- $[\text{Ru}(\text{L})(\text{bpy})_2](\text{ClO}_4)_2$ complex. The antibacterial study showed that the Ru(II) complexes (**1** and **2**) have better activity than the standard antibiotics but weak activity than the ligands.

ARTICLE HISTORY

Received 1 June 2016
Accepted 16 May 2017

KEYWORDS

Ruthenium(II) complex;
Schiff base; DNA and BSA
interaction; antibacterial
activity

Introduction

The chemistry of metal complexes with multidentate ligands and delocalized π -orbitals such as Schiff bases^[1,2] has attracted much attention because they act as a versatile model of metallic biosites.^[3] Schiff bases are reagents which are becoming increasingly important in the pharmaceutical, dye and plastic industries as well as for liquid crystal technology.^[4–7] Furthermore, Schiff bases enhance the solubility and stability of either homogeneous or heterogeneous catalysts.^[8] Schiff base compounds have been regarded as excellent fluorescent materials because of their ability

CONTACT Pabitra Chattopadhyay  pabitracc@yahoo.com  Department of Chemistry, Burdwan University, Golapbag, Burdwan-713104, India.

Color versions of one or more of the figures in the article can be found online at www.tandfonline.com/Incn.

© 2017 Taylor & Francis Group, LLC

to achieve high thermal stability as well as high photoluminescent efficiently. Transition metal complexes of these Schiff bases are also important not only due to the interesting structural and bonding modes they possess, but also because of their various industrial applications.^[9] Particularly, the use of ruthenium complexes to catalyze oxidation of alcohols by oxygen atom donors has been well documented.^[10,11]

The use of cinnamaldehyde to synthesis the Schiff base has been well established^[12] because cinnamaldehyde is effective in inhibiting growth of bacteria, yeast and filamentous molds. Antimicrobial activity of cinnamaldehyde is also attributed to its membrane action.^[13] Antifungal MICs of cinnamaldehyde are high and its use is further limited by its irritant effect on skin which is attributed to aldehyde function.^[14] Substituted cinnamaldehydes are known to be poorer skin sensitizer because they react slowly with amines.^[15]

Among the transition metals, the chemistry of ruthenium is currently receiving a lot of attention, primarily because of the fascinating electron transfer, photochemical and catalytic properties displayed by the complexes of this metal.^[16] Ruthenium(II) complexes with heterocyclic N-donor ligands have also been extensively investigated because of their interesting photochemical, catalytic, biological and electrochemical^[17-19] properties. Ruthenium-Schiff base complexes, containing oxygen and nitrogen as donor atoms were found to be very efficient catalysts in the oxidation of alcohols using N-methylmorpholine-N-oxide as co-oxidant.^[20-23]

As a part of our continuing efforts to synthesis and characterize ruthenium chelates using various types of N-donor ligands, in this paper, we describe the synthesis, characterization and DNA and protein binding studies of ruthenium(II) complexes.

Materials and methods

Reagents and measurements

All chemicals and reagents were obtained from commercial sources and used as received. Solvents were distilled from an appropriate drying agent. $\text{RuCl}_3 \cdot 3\text{H}_2\text{O}$ (Aldrich) was used without further purification. $[\text{Ru}^{\text{II}}(\text{bpy})_2\text{Cl}_2] \cdot 2\text{H}_2\text{O}$ was synthesized according to the literature method.^[24] *Tetra-n-butylammonium perchlorate* (TBAP) was prepared by addition of sodium perchlorate (taking the usual precaution of handling perchlorate salts!) to a hot solution of *tetra-n-butylammoniumbromide* (Aldrich).

The C, H, N elemental analyses were performed on a Perkin Elmer model 2400 elemental analyzer and ruthenium analyses were carried out by means of a Varian atomic absorption spectrophotometer (AAS) model-AA55B, GTA using graphite furnace. Electronic absorption spectra were recorded on a JASCO UV-Vis/NIR spectrophotometer model V-570 in the range of 1100–200 nm. IR spectra were recorded using a Perkin-Elmer FTIR model RX1 spectrometer (using KBr discs, $4000\text{--}300\text{ cm}^{-1}$). ^1H NMR spectra were recorded on a Bruker AC300 spectrometer using TMS as internal standard in CDCl_3 . Room temperature magnetic

susceptibility measurements were performed with a vibrating sample magnetometer PAR 155 model. Molar conductances (Λ_M) were measured in a Systronics conductivity meter (model 304) in acetonitrile with $\sim 10^{-3}$ mol L $^{-1}$ complex concentration. The measurement of pH of the reaction mixture was done with a systronics digital pH meter (Model 335). Electrochemical measurements were recorded on a CH-Instrument electrochemical system (Model 620D) using Pt-wire and Ag/AgCl as working and reference electrodes, respectively, with TBAP as supporting electrolyte. All the measurements were made at 298 K by using complex concentration of ca. 10^{-3} – 10^{-4} M in acetonitrile purged with dry nitrogen for 3–4 min in order to remove dissolved oxygen.

Preparation of the ligands

The syntheses of the ligands were carried out following the common procedure. The procedure for the preparation of *N,N'*-bis(4-nitrocinnamaldehyde)ethylenediamine (L^1) is here described in detail, being the other ligands obtained as solid products in the same way.

N,N'-Bis(4-nitrocinnamaldehyde)ethylenediamine (L^1): A solution of 4-nitrocinnamaldehyde (2 mmol) was added to an ice cooled methanolic solution of ethylenediamine (1 mmol). The mixture was then stirred for ≈ 3.0 h. A yellowish white coloured precipitate was obtained. The precipitate was filtered off and washed with 10 ml cold absolute methanol. The crude product was recrystallized from ethanol. The yield was 87%. The yield of the other ligand (L^2) was almost 90% following a similar method (Scheme 1). Yield: 87%. m.p. $215 \pm 1^\circ\text{C}$.

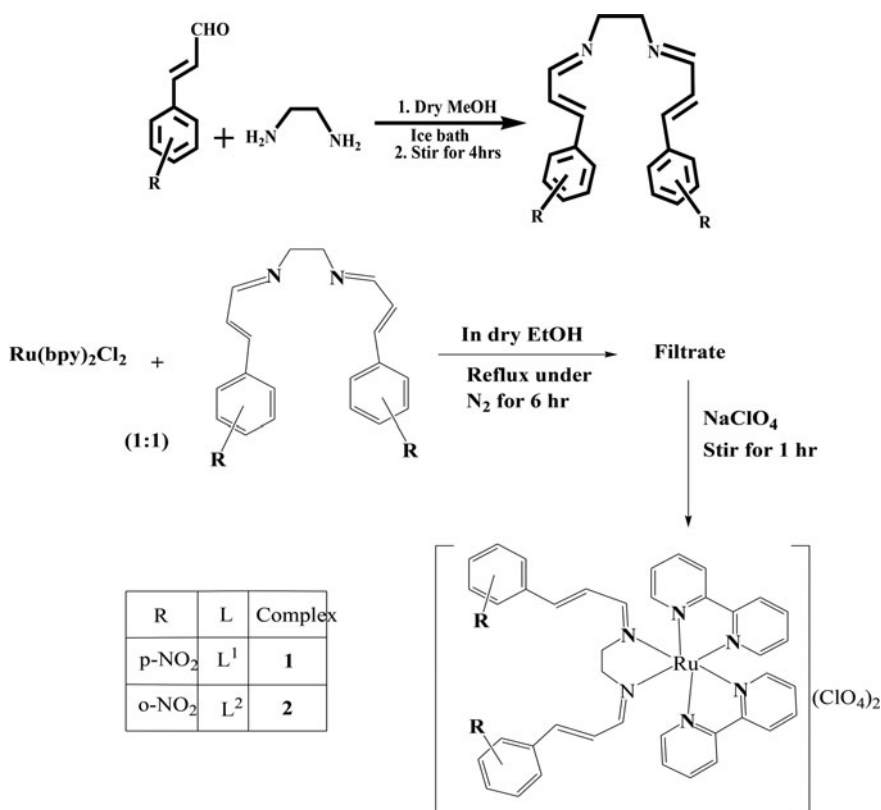
$\text{C}_{20}\text{H}_{18}\text{N}_4\text{O}_4$: Anal. Found: C, 63.48; H, 4.75; N, 14.81; Calc.: C, 63.34; H, 4.63; N, 14.61. IR (KBr, cm^{-1}): $\nu_{\text{C}=\text{N}}$, 1633. ^1H NMR (δ , ppm in CDCl_3): 8.11 (d, 4H, $j = 4.5$); 7.51 (m, 6H); 6.64 (d, 2H, $j = 8.53$); 5.326 (m, 2H); 1.073 (d, 4H, $j = 3.24$).

N,N'-Bis(2-nitrocinnamaldehyde)ethylenediamine (L^2): The ligand (L^2) was prepared taking 2-nitrocinnamaldehyde (2.0 mmol) instead of 4-nitrocinnamaldehyde following similar method as described above. Yield: 90%. m.p. $163 \pm 1^\circ\text{C}$.

$\text{C}_{20}\text{H}_{18}\text{N}_4\text{O}_4$: Anal. Found C, 63.22; H, 4.66; N, 14.78; Calc.: C, 63.34; H, 4.63; N, 14.61. IR (KBr, cm^{-1}): $\nu_{\text{C}=\text{N}}$, 1637. ^1H NMR (δ , ppm in CDCl_3): 8.043 (d, 2H, $j = 4.35$); 7.452 (m, 10H); 5.723 (d, 2H, $j = 4.3$); 1.102 (d, 4H, $j = 7.63$).

Preparation of $[\text{Ru}(\text{L}^1)(\text{bpy})_2](\text{ClO}_4)_2$ (1) and $[\text{Ru}(\text{L}^2)(\text{bpy})_2](\text{ClO}_4)_2$ (2)

Syntheses of the complexes were performed following a common procedure. To the ethanolic solution of L^1 (0.378 g, 1.0 mmol) in case complex 1 or L^2 (0.378 g, 1.0 mmol) complex 2, a solution of $[\text{RuCl}_2(\text{bpy})_2]$ (bpy = bipyridyl) (0.484 g, 1 mmol) in dry EtOH (20 mL) previously purged with N_2 was added dropwise and the resulting solution was refluxed for ~ 6 h under N_2 atmosphere. The solvent of the resulting solution was reduced to one-third of the total volume, and water solution of NaClO_4 (0.140 g 1mmol) was added in stirring condition. The resulting mixture was stirred for ~ 2 h and then by filtering a red solid mass was obtained. The product



Scheme 1. Synthetic procedure of organic moieties L and ruthenium(II) complexes.

was dissolved in the minimum amount of dichloromethane and chromatographed over a silica gel column prepared in dichloromethane. Only one band was obtained (Scheme 1).

[Ru(L¹)(bpy)₂](ClO₄)₂ (**1**): C₄₀H₃₄N₈RuCl₂O₁₂: Anal. Found: C, 48.42; H, 3.48; N, 11.11, Ru, 10.28 Calc.: C, 48.48; H, 3.43; N, 11.31, Ru, 10.20. IR (KBr cm⁻¹): ν_{C=N}, 1597; ν_(ClO₄-), 1107 and 623. Conductance Δ_o (ohm⁻¹ cm² mol⁻¹) in methanol: 52. ¹H NMR (δ, ppm in CDCl₃): 8.748 (d, 4H, j = 4.7); 8.741 (d, 4H, j = 5.1); 7.725 (m, 4H); 7.306 (t, 2H); 7.234 (m, 6H); 7.114 (m, 6H); 6.828 (m, 2H); 6.415 (d, 2H, j = 6.8; 1.153 (t, 4H). Yield: 70%.

[Ru(L²)(bpy)₂](ClO₄)₂ (**2**): C₄₀H₃₄N₈RuCl₂O₁₂: Anal. Found: C, 48.34; H, 3.40; N, 11.03, Ru, 10.18 Calc.: C, 48.48; H, 3.43; N, 11.31, Ru, 10.20. IR (KBr cm⁻¹): ν_{C=N}, 1599; ν_(ClO₄-), 1098 and 624. Conductance Δ_o (ohm⁻¹ cm² mol⁻¹) in methanol: 51. ¹H NMR (δ, ppm in CDCl₃): 8.001 (d, 4H, j = 5.2); 7.702 (d, 4H, j = 4.6); 7.633 (t, 4H); 7.455 (m, 8H); 7.360–7.263 (m, 6H); 6.868 (m, 2H); 6.305 (d, 2H, j = 9.8); 0.857(t, 4H). Yield: 63%.

DFT calculation

Full geometry optimization was carried out using the density functional theory method at the B3LYP level for **1** and **2**.^[25] All elements except ruthenium were assigned the 6–31G(d) basis set. The SDD basis set with effective core potential

was employed for the ruthenium atom.^[26] The vibrational frequency calculations were performed to ensure that the optimized geometries represent the local minima and there are only positive eigen values. All calculations were performed with Gaussian03 program package. Vertical electronic excitations based on B3LYP optimized geometry was computed using the time-dependent density functional theory (TD-DFT) formalism^[27] in acetonitrile using conductor-like polarizable continuum model (CPCM). Gauss Sum^[28] was used to calculate the fractional contributions of various groups to each molecular orbital.

DNA binding experiments

The tris-HCl buffer solution (pH 7.4), used in all the experiments involving CT-DNA, was prepared by using deionized and sonicated HPLC grade water (Merck). The used CT-DNA was sufficiently free from protein, being the ratio of UV absorbance of the DNA in tris-HCl solution at 260 and 280 nm (A_{260}/A_{280}) of *ca.* 1.9.^[29] The concentration of DNA was determined with the help of its extinction coefficient ϵ of $6600 \text{ L mol}^{-1} \text{ cm}^{-1}$ at 260 nm.^[30] The stock solution of DNA was always stored at 4°C and used within 4 days. Concentrated stock solution of complex was prepared by dissolving the ruthenium (II) complex in DMSO and suitably diluting with tris-HCl buffer to the concentration required for all the experiments. Absorption spectral titration experiment was performed by keeping constant the concentration of the ruthenium (II) complex while varying the CT-DNA concentration. To eliminate the absorbance of DNA itself, an equal solution of CT-DNA was added both to the ruthenium (II) complex solution and to the reference one.

In the fluorescence displacement experiment with ethidium bromide (EB), 5 μL of EB solution (1.0 mmol L^{-1}) in tris-HCl were added to 1.0 mL of DNA solution at saturated binding levels^[31] and stored in the dark for 2.0 h. The ruthenium (II) complex solution was titrated into the DNA/EB mixture and then diluted in tris-HCl buffer to 5.0 mL, making the solutions with the varied mole ratio of the metal complex to CT-DNA. Prior to measurements, the mixture was shaken up and incubated at room temperature for 30 min. The fluorescence spectra of EB bound to DNA were obtained at an emission wavelength of 584 nm. The viscosity values of the solutions were calculated from the observed flow time of CT-DNA-containing solution corrected from the flow time of buffer alone (t_0), $\eta = t - t_0$.^[32] The calculated data were used to plot the $(\eta/\eta_0)^{1/3}$ versus the ratio of the concentration of **1** and CT-DNA, where η is the viscosity of CT-DNA in the presence of the compound and η_0 is the viscosity of CT-DNA alone.

Protien (bovine serum albumin) binding experiments

Samples for spectroscopic measurements were prepared by dissolving bovine serum albumin in water and administering the appropriate concentration of the Ru(II) complexes. The samples were carefully degassed using pure nitrogen gas for 15 min. Quartz cells with high vacuum Teflon stopcocks were used for degassing.

Cyclic voltammetry (CV) experiments

Voltammetric measurements were carried out in a one-compartment cell using a glassy carbon (area, 0.088 cm²) or a Pt disk (area, 0.023 cm²) working electrode, a Pt flag counter electrode, and a Ag/AgCl reference electrode (SCE). Typical CV curves for 0.1 mM complexes in tris-buffer, in the absence and in the presence of CT DNA were carried out.

In vitro antibacterial assay

The biological activities of synthesized ligands (L¹ and L²) and the Ru (II) complexes have been studied for their antibacterial activities by agar well diffusion method.^[33–35] The antibacterial activities were done at 100 µg/mL concentrations of different compounds in DMF solvent by using four pathogenic gram negative bacteria (*Escherichia coli*, *Vibrio cholerae*, *Streptococcus pneumoniae*, *Shigella* spp) and one gram positive pathogenic bacteria (*Cereus bacillus*). Stock cultures of the test bacterial species were maintained on Nutrient Agar media by sub culturing in slants. The media were prepared by adding beef extract 3 g, peptone 5 g, agar 15 g, distilled water 1000 ml and the pH was adjusted at 7.2. Media was sterilized in the autoclave at 15 lbs pressure for 20 min. 20 mL of media was poured in each Petri dish and allowed to solidify. After solidification, nutrient agar plates were swabbed by sterile cotton swabs with 12 h old 0.1 ml broth culture of respective bacteria. The wells were bored with corkborer and the agar plugs were removed. Then solution of ligands and the Ru(II) complexes were added to the agar wells. DMF was used as a negative control. The Petri dishes were incubated at 37°C for 24 h. After incubation plates were observed for the growth inhibition zones. The diameter of the zone of inhibition was measured in millimeters. The well diameter was deducted from the zone diameter to get the actual zone of the inhibition and the values have been tabulated in Table 2.

Result and discussion

Synthesis and characterization

The organic moiety was synthesized by stirring *p/o-nitrocinnamaldehyde* and ethylenediamine in 2:1 ratio in methanol in an ice bath for ~3 h (Scheme 1). The yellowish white compound (L) *N,N'-bis(p/o-nitrocinnamaldehyde)ethylenediamine*

Table 1. UV-vis spectral data, electrochemical data^a.

Compd.	λ nm (ε) (ε, dm ³ .mol ⁻¹ .cm ⁻¹)	Electrochemical data E _{1/2} , ΔE (V) for Ru(II)/Ru(III)
1	473 (2354), 335 (13743), 241 (14143)	0.797 (0.159)
2	456 (2475), 339 (13547), 246 (14063)	0.935 (0.122)

^aIn acetonitrile.

Table 2. Antibacterial data of the ligands and Ru(II) complexes (100 µg/ml).

Treatment	Inhibition zone in mm				
	<i>E. coli</i>	<i>V. cholerae</i>	<i>S. pneumoniae</i>	<i>Cereus bacillus</i>	<i>Shigella sp.</i>
DMF(control)	0	0	0	0	0
L¹	16	12	12	14	17
1	20	18	16	16	22
L²	14	16	15	12	14
2	22	20	19	18	21
Bore diameter	06	06	06	06	06
Ampicillin	26	28	24	22	28

was obtained as the end product. The structural analysis by spectroscopic tools confirmed the product. These organic moieties act as bidentate N,N chelators.

The complexes **1** and **2** were obtained in good yield from the reaction of the $[\text{RuCl}_2(\text{bpy})_2]$ ($\text{bpy} = \text{bipyridyl}$) with equimolar amount of the organic moiety (L^1 , L^2) in dry EtOH medium in refluxing condition under dinitrogen (N_2) atmosphere followed by the addition of water solution of sodium perchlorate to the reaction mixture at cold condition (Scheme 1).

Neutral complexes **1** and **2** are soluble in DCM, acetonitrile, methanol, and DMF. Microanalytical data confirms the formulation of complexes **1** and **2**. The conductivity measurements indicate that both the ruthenium (II) complex species are non-electrolytes in methanolic solution and the magnetic moment studies demonstrate that the complexes are diamagnetic in nature.

DFT computations: Explanation of spectral and redox properties

DFT calculations have been performed for both **1** and **2**. The optimized structures of these molecules are developed using GAUSSIAN 03 (Figure 1). The calculated bond angles and lengths for **1** and **2** are given in Table 3. The orbital

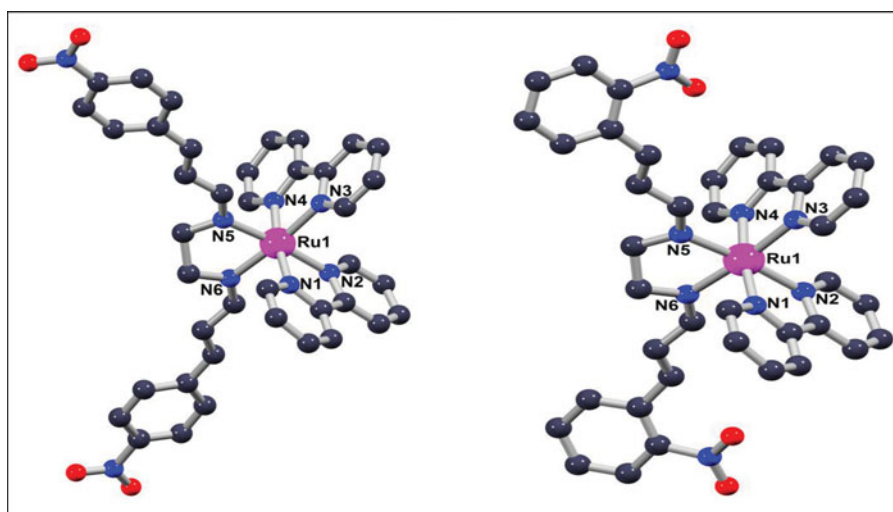
**Figure 1.** Optimized structure of **1** and **2** at DFT-B3LYP/6–31G(d) level of theory.

Table 3. Some selected optimized bond distances (Å) and angles (°) of **1** and **2**.

Bonds		
Ru1-N1	2.104	2.104
Ru1-N2	2.105	2.104
Ru1-N3	2.105	2.104
Ru1-N4	2.105	2.104
Ru1-N5	2.109	2.109
Ru1-N6	2.110	2.109
Angles		
N1-Ru1-N2	77.87	77.86
N1-Ru1-N3	97.13	97.41
N1-Ru1-N4	173.1	173.4
N1-Ru1-N5	97.18	97.55
N1-Ru1-N6	88.18	87.51
N2-Ru1-N3	89.65	90.48
N2-Ru1-N4	97.13	97.41
N2-Ru1-N5	173.7	173.6
N2-Ru1-N6	94.80	94.44
N3-Ru1-N4	77.87	77.86
N3-Ru1-N5	94.80	94.44
N3-Ru1-N6	173.7	173.6
N4-Ru1-N5	88.11	87.51
N4-Ru1-N6	97.18	97.55
N5-Ru1-N6	81.11	80.92

energies along with contributions from the ligands and metal are given in [Table 4](#) and [Figure 2](#), which depict selected occupied and unoccupied frontier orbitals for **1**. The HOMO of **1** is constituted by 39% contribution from L, whereas to HOMO-2 bpy contributes 17% and the metal ion 78%. The LUMO-2 is composed of L by 90%. Thus, HOMO \rightarrow LUMO is considered as major transition corresponding to $d\pi(\text{Ru}) / \pi(\text{L}^1) \rightarrow \pi^*(\text{bpy})$. The other transitions are HOMO-1 \rightarrow LUMO+1

Table 4. Energy and composition of some selected MOs of **1**.

MO	Energy (eV)	% of Composition		
		Ru	L ¹	Bpy
LUMO+10	- 5.01	33	09	58
LUMO+9	- 5.52	02	96	02
LUMO+8	- 5.55	02	97	01
LUMO+7	- 6.22	01	01	98
LUMO+6	- 6.24	05	01	94
LUMO+5	- 6.32	03	01	96
LUMO+4	- 6.52	02	02	96
LUMO+3	- 7.17	03	93	04
LUMO+2	- 7.25	05	90	05
LUMO+1	- 7.31	05	05	90
LUMO	- 7.37	02	05	93
HOMO	- 10.62	54	39	07
HOMO -1	- 10.63	50	43	07
HOMO -2	- 10.88	78	05	17
HOMO -3	- 11.24	0	100	0
HOMO -4	- 11.24	0	100	0
HOMO -5	- 11.37	26	68	06
HOMO -6	- 11.42	02	97	01
HOMO -7	- 11.43	01	99	0
HOMO -8	- 11.47	24	70	06
HOMO -9	- 11.62	0	100	0
HOMO -10	- 11.62	0	100	0

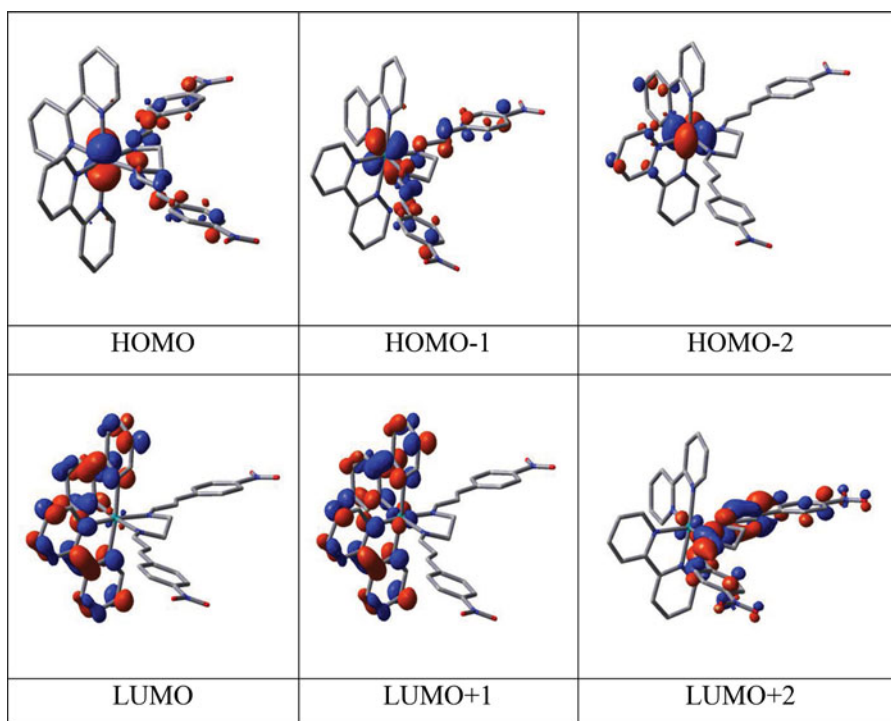


Figure 2. Contour plots of some selected MOs of **1**.

[$d\pi(\text{Ru}) / \pi(\text{L}^1) \rightarrow \pi^*(\text{bpy})$], HOMO-1 \rightarrow LUMO [$d\pi(\text{Ru}) / \pi(\text{L}^1) \rightarrow \pi^*(\text{bpy})$], and HOMO-2 \rightarrow LUMO+2 [$d\pi(\text{Ru}) \rightarrow \pi^*(\text{L}^1)$] that are intra-ligand and ligand-to-ligand charge transfer transitions. All these transitions are observed for **1**, and the calculated transitions are reported in Table 5. Solvent polarity stabilizes occupied MO's more efficiently than unoccupied MO's. Thus, the energy separation (DE) between HOMO and LUMO increase on going from gas phase to MeCN solution.

Figure 3 depicts selected occupied and unoccupied frontier orbitals of **2**. The metal significantly contributes to the occupied MO's (76%, comparable to 78% of **1**). Bipyridine contributes 18% to HOMO-2 and 94% to LUMO in **2**. The orbital energies of **2** along with contributions from the ligands and metal are given in Table 6

Table 5. Calculated vertical electronic transitions of **1**.

E_{ex} (eV)	λ_{ex} (nm)	Osc. Strength (f)	Key transitions	Character	$\lambda_{\text{expt.}}$ ($\text{M}^{-1} \text{cm}^{-1}$)
2.2703	546.1	0.1160	(85%) HOMO \rightarrow LUMO	$d\pi(\text{Ru}) / \pi(\text{L}^1) \rightarrow \pi^*(\text{bpy})$	
2.4476	506.6	0.2505	(74%) HOMO-1 \rightarrow LUMO+1	$d\pi(\text{Ru}) / \pi(\text{L}^1) \rightarrow \pi^*(\text{bpy})$	
2.5467	486.8	0.2899	(38%) HOMO-1 \rightarrow LUMO (31%) HOMO \rightarrow LUMO+1	$d\pi(\text{Ru}) / \pi(\text{L}^1) \rightarrow \pi^*(\text{bpy})$	473(2354)
2.8452	435.8	0.1543	(71%) HOMO-2 \rightarrow LUMO+2	$d\pi(\text{Ru}) \rightarrow \pi^*(\text{L}^1)$	
3.6209	342.4	0.1878	(61%) HOMO-1 \rightarrow LUMO+5	$d\pi(\text{Ru}) / \pi(\text{L}^1) \rightarrow \pi^*(\text{bpy})$	
3.6566	339.1	0.5318	(69%) HOMO-3 \rightarrow LUMO	$\pi(\text{L}^1) \rightarrow \pi^*(\text{bpy})$	335(13743)
3.7443	331.1	0.1021	(77%) HOMO-2 \rightarrow LUMO+6	$d\pi(\text{Ru}) \rightarrow \pi^*(\text{bpy})$	
3.7506	330.57	0.1279	(55%) HOMO-4 \rightarrow LUMO (21%) HOMO-5 \rightarrow LUMO	$d\pi(\text{Ru}) / \pi(\text{L}^1) \rightarrow \pi^*(\text{bpy})$	
3.7727	328.63	0.1781	(76%) HOMO-4 \rightarrow LUMO+1	$\pi(\text{L}^1) \rightarrow \pi^*(\text{bpy})$	

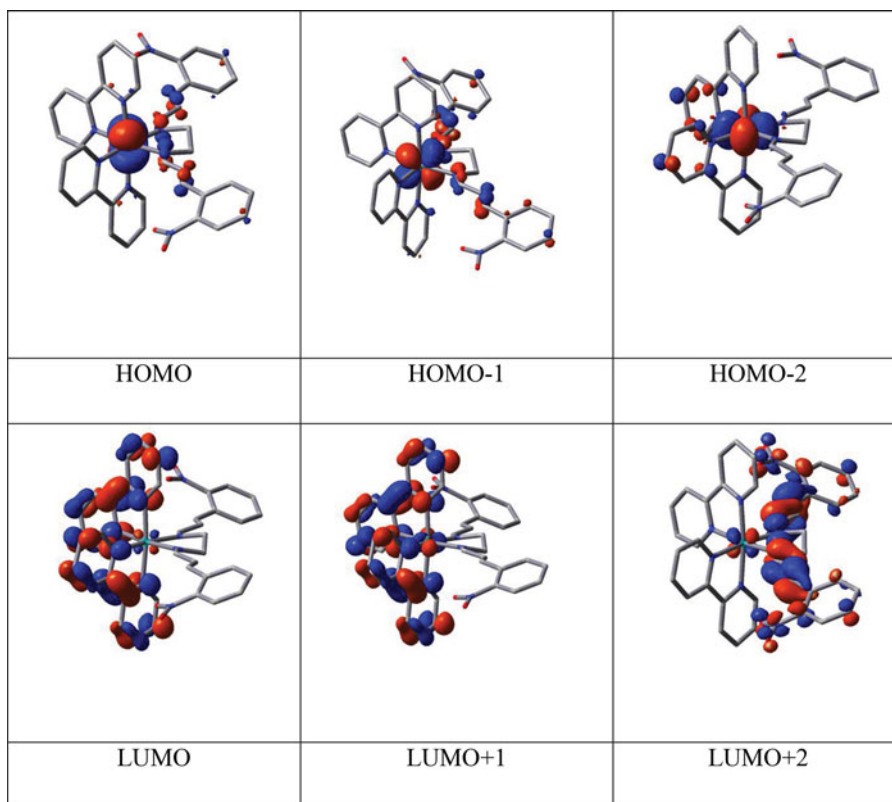


Figure 3. Contour plots of some selected MOs of **2**.

Table 6. Energy and composition of some selected MOs of **2**.

MO	Energy (eV)	% of Composition		
		Ru	L ²	bpy
LUMO+10	-4.68	36	06	58
LUMO+9	-4.8	37	15	48
LUMO+8	-5.94	04	08	88
LUMO+7	-5.96	01	01	98
LUMO+6	-6.04	01	66	33
LUMO+5	-6.06	01	93	06
LUMO+4	-6.09	04	26	70
LUMO+3	-6.26	02	08	90
LUMO+2	-6.85	03	97	0
LUMO+1	-6.92	05	04	91
LUMO	-7.05	06	0	94
HOMO	-10.45	67	25	08
HOMO -1	-10.48	59	32	09
HOMO -2	-10.64	76	06	18
HOMO -3	-11.25	15	81	04
HOMO -4	-11.3	14	82	04
HOMO -5	-11.45	0	100	0
HOMO -6	-11.45	0	100	0
HOMO -7	-11.8	02	96	02
HOMO -8	-11.81	02	95	03
HOMO -9	-11.93	01	03	96
HOMO -10	-11.96	02	03	95

Table 7. Calculated vertical electronic transitions of **2**.

E_{ex} (eV)	λ_{ex} (nm)	Osc. Strength (f)	Key transitions	Character	$\lambda_{\text{expt.}}$ ($M^{-1} \text{ cm}^{-1}$)
2.4463	506.8	0.0985	(83%)HOMO→LUMO	$d\pi(\text{Ru}) \rightarrow \pi^*(\text{bpy})$	456 (2475)
2.5793	480.68	0.1365	(60%)HOMO→LUMO+2 (31%)HOMO-1→LUMO+1	$d\pi(\text{Ru}) \rightarrow \pi^*(L^2)$ $d\pi(\text{Ru}) \rightarrow \pi^*(\text{bpy})$	
2.5957	477.65	0.2064	(56%)HOMO-1→LUMO+1 (28%)HOMO→LUMO+2	$d\pi(\text{Ru}) \rightarrow \pi^*(\text{bpy})$ $d\pi(\text{Ru}) \rightarrow \pi^*(L^2)$	
2.8332	437.61	0.1522	(74%)HOMO-2→LUMO+2 (20%)HOMO-1→LUMO+3	$d\pi(\text{Ru}) \rightarrow \pi^*(L^2)$ $d\pi(\text{Ru}) \rightarrow \pi^*(\text{bpy})$	
3.2556	380.83	0.1605	(45%)HOMO-2→LUMO+4 (45%)HOMO-1→LUMO+5	$d\pi(\text{Ru}) \rightarrow \pi^*(\text{bpy})$ $d\pi(\text{Ru}) \rightarrow \pi^*(L^2)$	
3.7183	333.44	0.3660	(42%)HOMO-2→LUMO+6 (33%)HOMO-3→LUMO	$d\pi(\text{Ru}) \rightarrow \pi^*(L^2)$ $\pi(L^2) \rightarrow \pi^*(\text{bpy})$	339 (3547)

and the calculated transitions are in Table 7. The intensity of these transitions has been assessed from oscillator strength (f). In MeCN, the longest wavelength band is calculated at 546.1 nm (f, 0.1160) for **1** followed by transitions at 506.6 (f, 0.2505), 486.2 (f, 0.2899), and 435.8 (f, 0.1543) nm along with a large number of transitions in the UV region (<400 nm). In **2**, the calculated transitions are 506.8 (f, 0.0985), 480.68 (f, 0.1365), 477.65 (f, 0.2064), and 437.61 (f, 0.1522) nm. The observed transitions are in agreement with the calculated ones for both complexes.

Spectral properties

Infrared spectral studies

The IR spectra of the complexes are compared with the free ligands in order to confirm the ligand coordination to the metal, and for this there are some reference peaks that are of good help for achieving this goal. The $\nu_{\text{C=N}}$ band in the free ligand, L^1 is 1633 cm^{-1} and it is shifted to lower wave numbers in the complex **1**, suggesting coordination to the metal ion. The similar result obtained for **2**. The characteristic bands at $1595\text{--}1600 \text{ cm}^{-1}$ is assigned to $\nu(\text{C=N})$ of the coordinated ligands (L^1/L^2) in the complexes. As we know, in going from $-\text{C=N}-(\sigma^2\pi^2)$ to $(\sigma^2\pi^2\pi^*)$, the bond order decreases from 2 to 1.5; therefore, it was observed that the vibrational frequency of $\nu_{\text{C=N}}$ decreases significantly from the free ligand value ($1630\text{--}1640 \text{ cm}^{-1}$). The complexes $[\text{Ru}(\text{L})(\text{bpy})_2](\text{ClO}_4)_2$ show sharp absorption bands around 1107 cm^{-1} and 623 cm^{-1} assignable to $\nu_{\text{s}(\text{ClO}_4^-)}$ and $\nu_{\text{as}(\text{ClO}_4^-)}$, which are absent in the spectra of the free organic moieties (L^1 and L^2).

$^1\text{HNMR}$ spectra

The $^1\text{HNMR}$ spectra of the organic moieties and the $[\text{Ru}(\text{L})(\text{bpy})_2](\text{ClO}_4)_2$ complexes were recorded in CDCl_3 . The characteristic signals for the protons of L^1 and L^2 appeared in the spectra as usual fashion in support of the proposed structural formulas. In the ^1H NMR spectrum of the complexes the protons appeared at characteristic δ values and these values are in accordance with the proposed structure. It

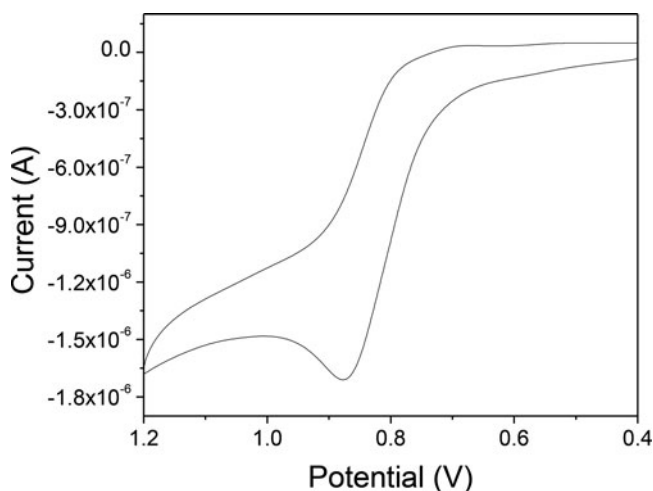


Figure 4. Cyclic voltammogram of complex **1** in MeCN (0.1 M *n*-Bu₄NClO₄) at 298 K, Ag/AgCl reference electrode, and scan rate 400 mV/s.

was observed that characteristic signals for the protons of the complexes appeared at higher δ values with respect to the free organic moieties.

Electronic absorption spectra

The electronic absorption spectra of the complexes were recorded at room temperature using acetonitrile as the solvent and data are reported in Table 1. The spectra of the complexes exhibit the characteristic transitions in the range of 240–245 nm and 335–340 nm corresponding to intramolecular $\pi \rightarrow \pi^*$ and $n \rightarrow \pi^*$ transitions, respectively. A band at 473 and 456 nm in **1** and **2**, respectively, were observed due to the $d(\text{Ru}) \rightarrow \pi^*$ (ligand) MLCT transitions.

Electrochemical behavior

The redox properties of the complexes were examined by cyclic voltammetry using a Pt-disk working electrode, a Pt-wire auxiliary electrode and Ag/AgCl electrode as a reference electrode in dry MeCN using [*n*-Bu₄N]ClO₄ (0.1 M) as the supporting electrolyte. Voltammetric data are given in Table 1. Each complex exhibits a quasi-reversible Ru^{II}/Ru^{III} redox couple around a redox wave at *ca.* $E_{1/2}$ of 0.797 V (versus Ag/AgCl) for **1** (Figure 4) and at *ca.* $E_{1/2}$ of 0.935 V (versus Ag/AgCl) for **2** in MeCN solution at 25°C. No cathodic response for Ru^{II} \rightarrow Ru^I reduction was obtained for the complexes up to -1.50 V. The voltammetric parameters were studied in the scan rate interval 50–400 mV s⁻¹. The ratio between the cathodic peak current and the square root of the scan rate ($I_{pc} / \nu^{1/2}$) is approximately constant. The peak potential shows a small dependence on the scan rate. The ratio I_{pc} to I_{pa} is close to unity. From these data, it can be concluded that the redox couple is related to a quasi-reversible one-electron transfer process controlled by diffusion.

DNA-binding studies

The binding interaction of the Ru (II) complex **1** (complex **2** give same groove binding interaction) with calf thymus DNA (CT-DNA) has been investigated by using absorption and emission spectra.

Spectrophotometric study

Electronic absorption spectroscopy is an effective method to examine the binding modes of metal complexes with DNA. In general, binding of the ruthenium (II) complex to the CT-DNA helix is examined by an increase of the absorption band (*ca.* 304 nm) of ruthenium (II) complex. This increasing absorbance indicates that there is the involvement of strong interactions between complex and the base pairs of DNA. The absorption spectra of the Ru (II) complex **1** in the absence and presence of CT-DNA are given in (Figure 5). The spectral change might be interpreted as due to the groove binding nature of the adducts^[36] since ruthenium (II) complexes containing Schiff base ligands, which likely facilitates the formation of Vander-Waals contacts or hydrogen bonds during interaction with DNA grooves. In order to further illustrate the binding strength of the Ru(II) complex with CT-DNA, the intrinsic binding constant K_b was determined from the spectral titration data using the following equation^[37]

$$[\text{DNA}] / (\varepsilon_a - \varepsilon_f) = [\text{DNA}] / (\varepsilon_b - \varepsilon_f) + 1 / [K_b (\varepsilon_b - \varepsilon_f)]$$

where [DNA] represents the DNA concentration, ε_f and ε_b are the extinction coefficients for the free and fully bound ruthenium(II) complex, respectively, and ε_a the metal complex extinction coefficient during each addition of DNA. The $[\text{DNA}] / (\varepsilon_a - \varepsilon_f)$ plot against [DNA] gave a linear relationship (Figure 6). The intrinsic binding

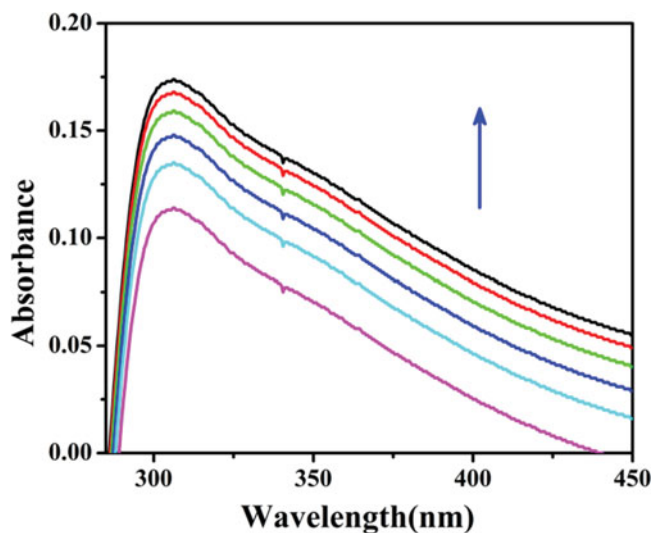


Figure 5. Electronic spectra of complex **1** through titration with CT-DNA in tris-HCl. The increase of DNA concentration is indicated by an arrow.

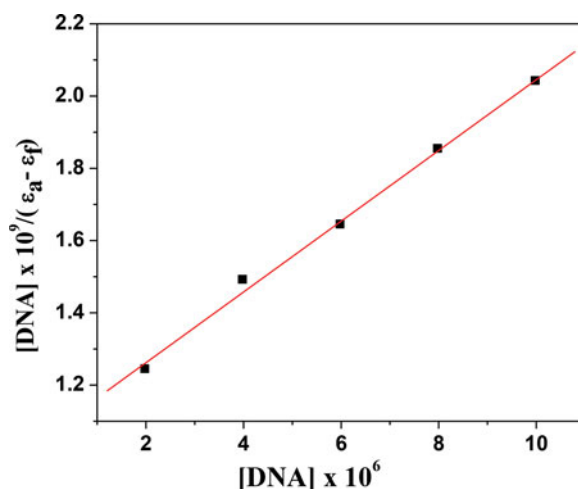


Figure 6. Plot of $[DNA]/(\epsilon_a - \epsilon_f)$ vs $[DNA]$ for the titration of CT-DNA with complex **1** in tris-HCl buffer; binding constant $K_b = 9.1866 \times 10^4 \text{ M}^{-1}$ ($R = 0.99798$ for five points).

constants (K_b) for the complex **1** were calculated from the slope to intercept ratio ($K_b = 9.1866 \times 10^4 \text{ M}^{-1}$, $R = 0.99798$ for five points). The value is in close agreement with those of the well-established groove binding rather than classical intercalation agent.^[38]

Spectrofluometric study

Fluorescence intensity of EB bound to CT-DNA at excitation wavelength of 522 nm shows a decreasing trend with the increasing concentration of the complex **1** (Figure 7). The quenching of EB bound to DNA by the complex **1** is in agreement with the linear Stern–Volmer equation^[39]

$$I_0/I = 1 + K_{sv} [Q]$$

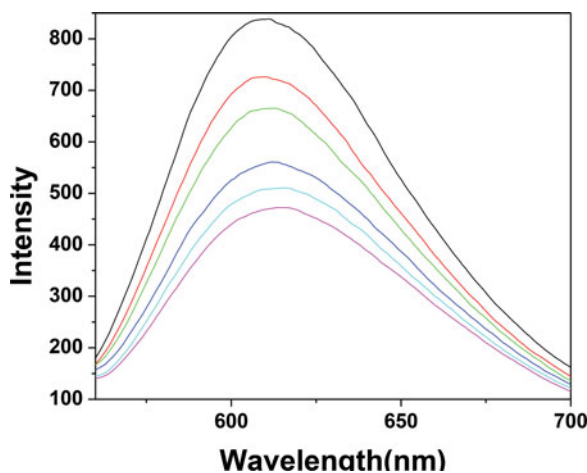


Figure 7. Emission spectra of the CT-DNA-EB system in tris-HCl buffer based on the titration of complex. $\lambda_{ex} = 522 \text{ nm}$.

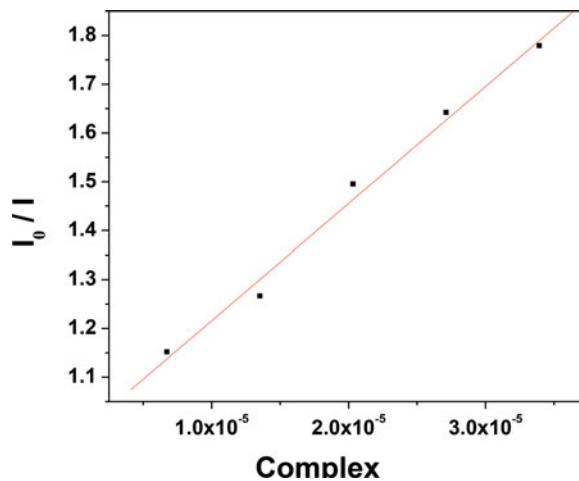


Figure 8. Plot of I_0/I vs [complex] for the titration of CT-DNA–EB system with complex **1** using spectrofluorimeter; linear Stern–Volmer quenching constant (K_{sv}) = 1.125×10^4 ; ($R = 0.99023$ for five points).

where I_0 and I represent the fluorescence intensities in the absence and presence of quencher respectively. K_{sv} is a linear Stern–Volmer quenching constant, Q is the concentration of quencher. The K_{sv} value calculated from the plot (Figure 8) of I_0/I versus [complex] for the complex **1** is 2.5×10^4 ($R = 0.99506$ for five points), suggesting a strong affinity of the complex **1** to CT-DNA. The value is in close agreement with those of the well-established groove binding rather than classical intercalation agent.^[40]

Number of binding sites can be calculated from fluorescence titration data using the following equation^[41]

$$\log [(I_0 - I) / I] = \log K + n \log [Q]$$

K and n is the binding constant and binding site of complex **1** to CT-DNA, respectively. The number of binding sites (n) determined from the slope of $\log[(I_0 - I)/I]$ versus $\log[Q]$ is 0.84 which indicates less association of the complex **1** to the number of DNA bases, also suggesting strong affinity of the complex **1** through surface or groove binding.

Viscosity technique

From spectroscopic technique it was observed that the complex **1** has a strong interaction with DNA, so to further clarify the interactions study between the complex and DNA, viscosity measurements were carried out. From this experiment it was observed that there is almost no effect on the relative viscosity of the DNA solution. This experiment suggests that the binding mode is groove binding which is in support of the above results obtained in spectroscopic study, otherwise if it be intercalative candidate, then the change of the relative viscosity of the DNA solution was

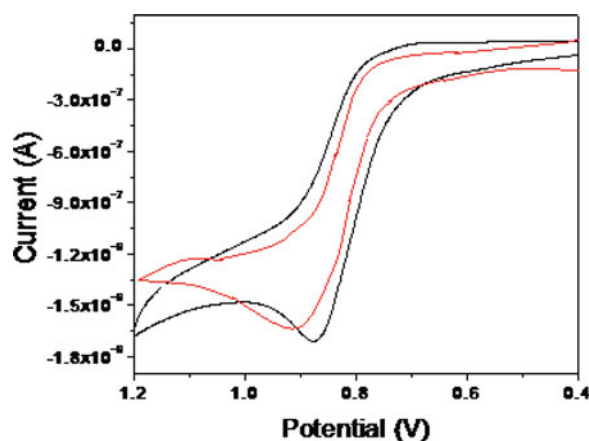


Figure 9. Cyclic voltammograms of the ruthenium (II) complex in Tris-HCl buffer in (a) absence (black colored curve) and (b) presence of CT-DNA (red colored curve).

observed because intercalation leads to an increase in the DNA viscosity by lengthening the DNA helix, or the non-classical intercalation could bend (or kink) the DNA helix and reduce its effective length and, concomitantly, its viscosity.^[42,43]

Electrochemical study

Electrochemical investigations are useful technique to analyze metal-DNA interactions over spectroscopic methods.^[44] The binding nature of the ruthenium(II) complex **1** with DNA, has been shown in (Figure 9). Cyclic voltammograms of complex **1**, in the absence and presence of CT-DNA, exhibited significant shifts in the anodic peak potentials followed by decrease in peak currents, indicating the interaction occurring between the metal complex and CT-DNA. The shift in the value of the formal potential (ΔE^0) is used to calculate the ratio of equilibrium binding constants K_{2+}/K_{3+} according to the following equation described by Bard and Carter.^[45]

$$\Delta E^{\circ} = E_b^{\circ} - E_f^{\circ} = 0.059 \log (K_{2+}/K_{3+})$$

where E_b° and E_f° are the formal potentials of the bound and free complex forms, respectively, and K_{2+} and K_{3+} are the corresponding binding constants for the binding of reduction and oxidation species to DNA, respectively. Ratio of equilibrium binding constants, K_{2+}/K_{3+} is calculated to be 2.55 that indicates a strong binding of DNA with reduced form of ruthenium complex, i.e., Ru(II) species.

Protien (bovine serum albumin) binding experiments

Absorption characteristics of BSA-Ru(II) complex 1

The absorption spectra of BSA in the absence and presence of Ru(II) complex **1** (complex **2** give same type of binding interaction) were studied at different concentrations (Figure 10). From this study we observed that absorption of BSA increases

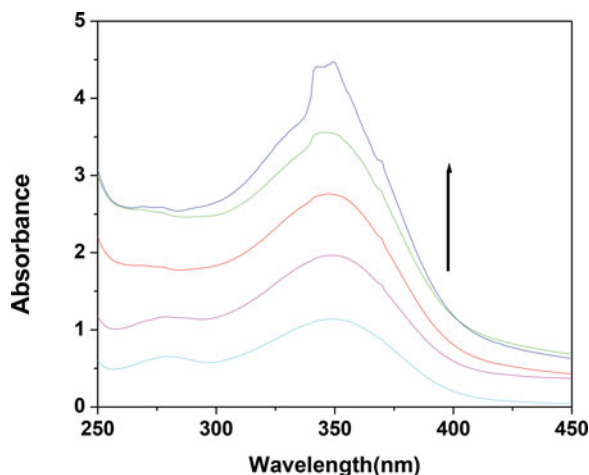


Figure 10. Absorption spectrum of BSA in the presence of complex in the concentration range 0–6.34 $\times 10^{-5}$ M.

regularly upon increasing the concentration of the complex. It may be due to the adsorption of BSA on the surface of the complex. From these data the apparent association constant (K_{app}) determined of the complexes with BSA has been determined using the following equation.^[37]

$$1/(A_{obs} - A_0) = 1/(A_c - A_0) + 1/K_{app} (A_c - A_0) [\text{comp}]$$

Where, A_{obs} is the observed absorbance of the solution containing different concentrations of the complex at 280 nm, A_0 and A_c are the absorbances of BSA and the complex at 280 nm, respectively, with a concentration of complex and K_{app} represents the apparent association constant. The enhancement of absorbance at 280 nm was due to absorption of the surface complex, based on the linear relationship between $1/(A_{obs} - A_0)$ vs reciprocal concentration of the complex with a slope equal to $1/K_{app}(A_c - A_0)$ and an intercept equal to $1/(A_c - A_0)$ (Figure 11). The value of the apparent association constant (K_{app}) for complex **1** determined from this plot is $6.12 \times 10^3 \text{M}^{-1}$ ($R = 0.99896$ for four points).

Fluorescence quenching of BSA by the complex 1

The effect of increasing the concentration of the complex on the fluorescence emission spectrum of BSA were studied and represented in (Figure 12). With the addition of complex BSA fluorescence emission is quenched. The fluorescence quenching is described by the Stern–Volmer relation^[39]:

$$I_0/I = 1 + K_{SV} [\text{complex}]$$

where I_0 and I represent the fluorescence intensities of BSA in the absence and presence of quencher, respectively. K_{SV} is the linear Stern–Volmer quenching constant and $[\text{complex}]$ the molar concentration of the quencher. A linear plot (Figure 13) between I_0/I against $[\text{complex}]$ was obtained and from the slope we calculated the

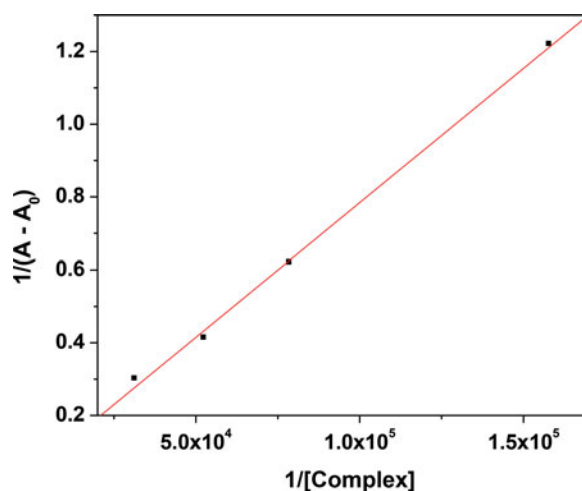


Figure 11. Plot of $1/(A - A_0)$ vs $1/[\text{Complex}]$ for the titration of BSA with complex **1** in tris HCl buffer; apparent association constant ($K_{\text{app}} = 6.12 \times 10^3 \text{M}^{-1}$) ($R = 0.99896$ for four points).

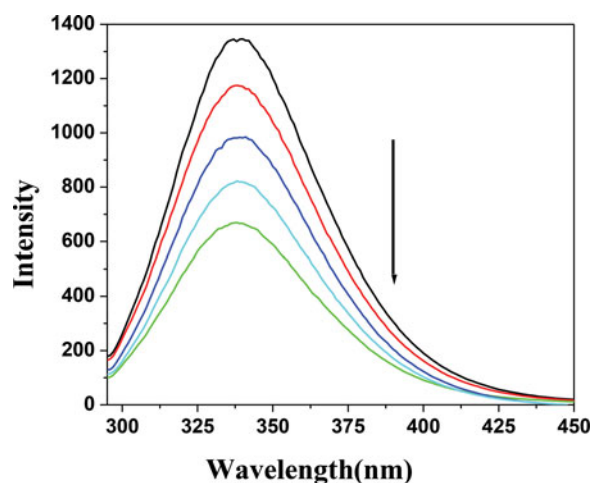


Figure 12. Fluorescence Quenching of BSA in the presence of complex **1** in the concentration range $0-3.17 \times 10^{-5} \text{M}$.

K_{SV} as 8.4×10^4 ($R = 0.99321$ for five points), suggesting a strong affinity of the complex **1** to BSA.

Antibacterial activity

The *in vitro* antimicrobial screening effects of the ligands (L^1 and L^2) and their ruthenium complexes (**1** and **2**) were performed against five pathogenic bacteria *viz.*, (*Escherichia coli*, *Vibrio cholerae*, *Streptococcus pneumoniae*, *Shigella* sp. and *Cereus bacillus*) by the agar disc diffusion method and the results are shown in [Table 2](#). The activities of the compounds were compared with standards Antibiotic such as ampicillin. The results indicate that the ruthenium (II) complexes are more active when compared with parent ligands, this would suggest that the chelation could facilitate

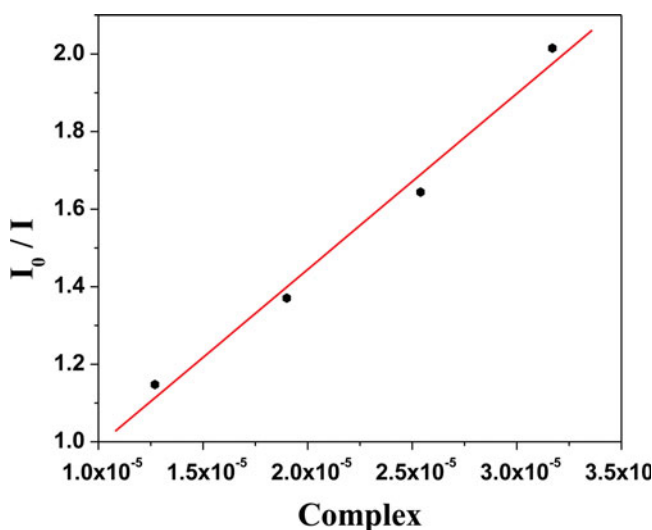


Figure 13. The Stern–Volmer plot, the linear Stern–Volmer quenching constant (K_{sv}) = 8.4×10^4 ($R = 0.99321$ for four points).

the ability of a complex to cross a cell membrane and can be explained by Tweedy's chelation theory.^[46] Such a chelation could enhance the lipophilic character of the central metal atom, which subsequently favors its permeation through the lipid layer of the cell membranes and blocks the metal binding sites in enzymes of microorganisms. However, the Ru(II) complexes (**1** and **2**) have better activity than the standard antibiotics.

Conclusions

In this article, we have presented the synthesis of two Schiff base ligands, $L^1 = N,N'$ -bis(4-nitrocinnamaldehyde)ethylenediamine and $L^2 = N,N'$ -bis(2-nitrocinnamaldehyde) ethylenediamine and their corresponding ruthenium(II) complexes. The ligands L^1 and L^2 and the complexes (**1** and **2**) have been characterized by IR, UV-Vis, NMR, electrochemical techniques and spectroscopic analysis. The aim of this research was devoted to study the interaction of the complexes with calf thymus DNA and BSA and the antibacterial activity of the complexes and the organic moieties. The interaction of the Ru (II) complexes with CT-DNA at physiological pH shows very good agreement between spectrophotometric and fluorimetric methods of measurement, the data lend support to the validity of the methods used in the experiments and all results indicate that the Ru (II) complexes bind to CT-DNA through surface or groove binding mode and it is also in accordance with the unchanged values of the viscosity of the DNA solution upon addition of complex **1**. This study clearly indicates that **1** binds to calf thymus DNA in a groove binding interaction^[47–49] but not in a intercalative mode like reported octahedral ruthenium (II) complexes.^[50–53] However, the K_b of **1** is comparable to that of the reported ruthenium (II) complexes.^[47–49] The electrochemical studies

indicated that the reduced form of the complex Ru(II) has a stronger association to DNA than the oxidized Ru(III) form. The absorption and emission spectroscopy, as well as fluorescence spectroscopy tools are also used to study the interaction of the complex **1** with bovine serum albumin that proves the formation of a ground state BSA-[Ru(L¹)(bpy)₂](ClO₄)₂ complex. From the antibacterial study it was observed that Ru(II) complexes are highly active than their parent ligands but lesser activity than standard antibiotic against pathogenic bacteria *viz.* (*Escherichia coli*, *Vibrio cholerae*, *Streptococcus pneumoniae*, *Shigella* sp. and *Cereus bacillus*).

Acknowledgment

Financial support from Council of Scientific and Industrial Research (CSIR), New Delhi, India is gratefully acknowledged.

References

1. Nakajima, K.; Kijima, K.; Kojima, M.; Fujita, T. Preparation and characterization of optically active schiff base-oxovanadium(IV) and -oxovanadium(V) complexes and catalytic properties of these complexes on asymmetric oxidation of sulfides into sulfoxides with organic hydroperoxides. *Bull. Chem. Soc. Jpn.* **1990**, *63*, 2620–2630.
2. Nakajima, K.; Ando, Y.; Mano, H.; Kojima, M. Inorg. Chim. Acta. Photosubstitution reactivity, crystal structures, and electrochemistry of ruthenium(II) (III) complexes containing tetradentate (O₂N₂, S₂N₂, and P₂N₂) Schiff base ligands. *Inorg. Chim. Acta.* **1998**, *274*, 184–191.
3. Casella, L.; Gullotti, M.; Vigano, R. Copper(II)-N₂S₂ complexes of the imines of 1-phenyl-3-formyl-2(1H)-pyridinethione. *Inorg. Chim. Acta.* **1986**, *121*, 124.
4. Wai Yeung, W.; Guo_Liang, L.; Ka_Fai, N. J. Organomet. Chem. Synthesis, structures and properties of platinum(II) complexes of oligothiophene-functionalized ferrocenylacetylene. *J. Chem. Soc. Dalton Trans.* **2001**, 3250–3260.
5. Reddy, B. J.; Frost, L. R.; Locke, A. Synthesis and spectroscopic characterisation of aurichalcite (Zn,Cu₂₊)⁵(CO₃)²(OH)₆; implications for Cu–ZnO catalyst precursors. *Trans. Met. Chem.* **2008**, *33*, 331–339.
6. Qi_Long, Z.; Bi_Xue, Z.; Leonard, F. L.; Gang, W. Dinuclear nickel(II) complex of a N₂O₃-donor Schiff base derived from acetylacetone and 1,3-diamino-2-hydroxypropane. *Inorg. Chem. Commun.* **2008**, *11*, 678–680.
7. Borisova, N. E.; Reshetova, M. D.; Magdesieva, T. V. Influence of ligands' peripheral substituents on the structure, magnetochemical and electrochemical behaviour of complexes containing a Cu₂O₂ butterfly core. *Inorg. Chim. Acta.* **2008**, *361*, 2032–2044.
8. Pal, S.; Pal, S. A diruthenium(III) complex possessing a diazine and two chloride bridges: synthesis, structure, and properties. *Inorg. Chem.* **2001**, *40*, 4807–4810.
9. Coucouvanis, D. The chemistry of the dithioacid and 1, 1-dithiolate complexes, 1968–1977. *Prog. Inorg. Chem.* **1979**, *26*, 301–489.
10. Sasmal, P. K.; Patra, A. K.; Chakraborty, A. R. Synthesis, structure, DNA binding and DNA cleavage activity of oxovanadium(IV) *N*-salicylidene-*S*-methylthiocarbamate complexes of phenanthroline bases. *J. Inorg. Biochem.* **2008**, *102*, 1463–1472.
11. Hassan, K.; Reza, A.; Sadegh, S. Synthesis, crystal structure and spectroscopic properties of some cadmium(II) complexes with three polyamine and corresponding macrocyclic Schiff base ligands. *J. Organomet. Chem.* **2008**, *693*, 2237–2243.

12. Shreaz, S.; Sheikh, R. A.; Bhatia, R.; Khan, N.; Sheikh, I.; Hashmi, A. A.; Manzoor, N.; Basir, S. F.; Khan, L. A. Antifungal activity of α -methyl trans cinnamaldehyde, its ligand and metal complexes: promising growth and ergosterol inhibitors. *Biometals*. **2011**, *24*, 923–933.
13. Bang, K. H.; Lee, D. W.; Park, H. M.; Rhee, Y. H. Inhibition of fungal cell wall synthesizing enzymes by trans-cinnamaldehyde. *Biosci. Biotechnol. Biochem.* **2000**, *64*, 1061–1063.
14. Wang, S. Y.; Chien, S. C.; Chang, S. T. Structure-activity relationships of cadinane-type sesquiterpene derivatives against wood-decay fungi. *Biores. Tech.* **2005**, *96*, 813–818.
15. Vimala, A. M.; Raymond, R. S. Mechanism of cinnamaldehyde sensitization. *Contact Dermat.* **1997**, *3*, 16–18.
16. Prasad, D. R.; Ferraudi, G. Excited-state redox properties of ruthenium(II) phthalocyanine from electron-transfer quenching. *J. Phys. Chem.* **1982**, *86*, 4037–4040.
17. Ghosh, B. K.; Chakravorty, A. Electrochemical studies of ruthenium compounds Part 1. Ligand oxidation levels. *Coord. Chem. Rev.* **1989**, *95*, 239–294.
18. Chen, H.; Perkinson, J. A.; Persons, S.; Coxall, R. A.; Gould, R. O.; Sadler, P. J. Organometallic ruthenium(II) diamine anticancer complexes: arene-nucleobase stacking and stereospecific hydrogen-bonding in guanine adducts. *J. Am. Chem. Soc.* **2002**, *124*, 3064–3082.
19. Banerjee, S.; Bhattacharya, S.; Dirghangi, B. K.; Menon, M.; Chakravorty, A. Chemistry of the rhenium-azopyridine family: an oxo parent and derivatives thereof including a novel oxo-imido dimer. *Inorg. Chem.* **2000**, *39*, 6–13.
20. Reimers, J. R.; Hush, N. S. Electron transfer and energy transfer through bridged systems. 4. Intermetallic coupling and electronic spectra of the bis(pentaammineruthenium) complexes of .alpha.,.omega.-dipyridyl trans-polyenes in deuterium oxide. *Inorg. Chem.* **1990**, *29*, 3686–3697.
21. Kureshy, R. I.; Khan, N. H.; Abdi, S. H. R. Enantioselective catalytic epoxidation of styrenes by iododisylbenzene using chiral ruthenium(II) Schiff base complexes. *J. Mol. Catal.* **1995**, *96*, 117–122.
22. Bhattacharya, S. 8-Quinolinolate complexes of ruthenium(ii). Synthesis, characterization and electron transfer properties. *Polyhedron*. **1993**, *12*, 235–239.
23. Bhowon, G.; Kam, L.; Wah, H.; Narain, R. Schiff base complexes of ruthenium(II) and their use as catalytic oxidant. *Polyhedron*. **1999**, *18*, 341–345.
24. Sullivan, B. P.; Salmon, D. J.; Meyer, T. J. Mixed phosphine 2,2'-bipyridine complexes of ruthenium. *Inorg. Chem.* **1978**, *17*, 3334–3341.
25. Lee, C.; Yang, W.; Parr, R. G. Development of the Colle-Salvetti correlation-energy formula into a functional of the electron density. *Phys. Rev. B.* **1988**, *37*, 785–789.
26. Fuentealba, P.; Preuss, H.; Stoll, H.; Szentpaly, L. V. A proper account of core-polarization with pseudopotentials: single valence-electron alkali compounds. *Chem. Phys. Lett.* **1982**, *89*, 418–422.
27. Casida, M. E.; Jamorski, C.; Casida, K. C.; Salahub, D. R. Molecular excitation energies to high-lying bound states from time-dependent density-functional response theory: characterization and correction of the time-dependent local density approximation ionization threshold. *J. Chem Phys.* **1998**, *108*, 4439–4449.
28. O'Boyle, N. M.; Tenderholt, A. L.; Langner, K. M. cclib: A library for package-independent computational chemistry algorithms. *J. Comput. Chem.* **2008**, *29*, 839–845.
29. Marmur, J. A procedure for the isolation of deoxyribonucleic acid from micro-organisms. *J. Mol. Biol.* **1961**, *3*, 208–218.
30. Reichmann, M. E.; Rice, S. A.; Thomas, C. A.; Doty, P. A further examination of the molecular weight and size of desoxypentose nucleic acid. *J. Am. Chem. Soc.* **1954**, *76*, 3047–3053.
31. Barton, J. K.; Goldberg, J. M.; Kumar, C. V.; Turro, N. J. Binding modes and base specificity of tris(phenanthroline)ruthenium(II) enantiomers with nucleic acids: tuning the stereoselectivity. *J. Am. Chem. Soc.* **1986**, *108*, 2081–2088.

32. Allardyce, C. S.; Dyson, P. J. Ruthenium in medicine: current clinical uses and future prospects. *Platinum. Met. Rev.* **2001**, *45*, 62–69.
33. Cordes, E. H.; Jencks, W. P. On the mechanism of Schiff base formation and hydrolysis. *J. Am. Chem. Soc.* **1962**, *84*, 832–837.
34. Chohan, Z. H.; Scozzafava, A.; Supuran, C. T. Zinc complexes of benzothiazole-derived Schiff bases with antibacterial activity. *J. Enzyme Inhib. Med. Chem.* **2003**, *18*, 259–263.
35. Sheikh, C.; Hossain, M. S.; Easmin, M. S.; Islam, M. S.; Rashid, M. Evaluation of in vitro antimicrobial and in vivo cytotoxic properties of some novel titanium-based coordination complexes. *Bio. Pharma. Bull.* **2004**, *27*, 710–713.
36. Kanthimathi, R. M.; Subramanian, V.; Nair, B. U. Interaction of DNA with [Cr(Schiff base)(H₂O)(2)]ClO₄. *Biochim. Biophys. Acta.* **2000**, *1475*, 157–162.
37. Pyle, A. M.; Rehmann, J. P.; Meshoyrer, R.; Kumar, C. V.; Turro, N. J.; Barton, J. K. Mixed-ligand complexes of ruthenium(II): factors governing binding to DNA. *J. Am. Chem. Soc.* **1989**, *111*, 3051–3058.
38. Streckowski, L.; Harden, D. B.; Wydra, R. L.; Stewart, K. D.; Wilson, W. D. Molecular basis for potentiation of bleomycin-mediated degradation of DNA by polyamines. Experimental and molecular mechanical studies. *J. Mol. Recog.* **1989**, *2*, 158–166.
39. Stern, O.; Volmer, M. über die Abklingzeit der Fluoreszenz. *Zeitschrift. fur. Physik.* **1919**, *20*, 183–188.
40. Streckowski, L.; Harden, D. B.; Wydra, R. L.; Stewart, K. D.; Wilson, W. D. Molecular basis for potentiation of bleomycin-mediated degradation of DNA by polyamines. Experimental and molecular mechanical studies. *J. Mol. Recog.* **1989**, *2*, 158–166.
41. Kathiravan, A.; Renganathan, R. Photoinduced interactions between colloidal TiO₂ nanoparticles and calf thymus-DNA. *Polyhedron.* **2009**, *28*, 1374–1378.
42. Satyanarayana, S.; Dabrowiak, J. C.; Chaires, J. B. Neither .DELTA.- nor .LAMBDA.-tris(phenanthroline)ruthenium(II) binds to DNA by classical intercalation. *Biochemistry.* **1992**, *31*, 9319–9324.
43. Satyanarayana, S.; Dabrowiak, J. C.; Chaires, J. B. Tris(phenanthroline)ruthenium(II) enantiomer interactions with DNA: mode and specificity of binding. *Biochemistry.* **1993**, *32*, 2573–2584.
44. Mahadevan, S.; Palaniandavar, M. Spectroscopic and voltammetric studies on copper complexes of 2,9-dimethyl-1,10-phenanthrolines bound to calf thymus DNA. *Inorg Chem.* **1998**, *37*, 693–700.
45. Carter, M. T.; Bard, A. J. Voltammetric studies of the interaction of tris(1,10-phenanthroline)cobalt(III) with DNA. *J. Am. Chem. Soc.* **1987**, *109*, 7528–7530.
46. Natarajan, K.; Poddar, R. K.; Agarwala, C. Mixed complexes of ruthenium(III) and ruthenium(II) with triphenylphosphine or triphenylarsine and other ligands. *J. Inorg. Nucl. Chem.* **1977**, *39*, 431–435.
47. Paul, H.; Mukherjee, T.; Drew, M.G.B.; Chattopadhyay, P. Synthesis, characterization, crystal structure, and DNA-binding of ruthenium(II) complexes of heterocyclic nitrogen ligands resulting from a benzimidazole-based quinazoline derivative. *J. Coord. Chem.* **2012**, *65*, 1289–1302.
48. Huang, H. L.; Li, Z. Z.; Wang, X. Z.; Liang, Z. H.; Liu, Y. J. Cytotoxicity, apoptosis, interaction with DNA, cellular uptake, and cell cycle arrest of ruthenium(II) polypyridyl complexes containing 4,4'-dimethyl-2,2'-bipyridine as ancillary ligand. *J. Coord. Chem.* **2012**, *65*, 3287–3298.
49. Paul, H.; Mukherjee, T.; Mukherjee, M.; Mondal, T. K.; Moirangthem, A.; Basu, A.; Zangrando, E.; Chattopadhyay, P. Ruthenium(II) complexes of pyrrolazo ligands: cytotoxicity, interaction with calf thymus DNA and bovine serum albumin. *J. Coord. Chem.* **2013**, *66*, 2747–2764.

50. Devi, C. S.; Satyanarayana, S. Review: Synthesis, characterization, and DNA-binding properties of Ru(II) molecular “light switch” complexes. *J. Coord. Chem.* **2012**, *65*, 474–486.
51. Guo, Q. F.; Liu, S. H.; Liu, Q. H.; Xu, H. H.; Zhao, J. H.; Wu, H. F.; Li, X. Y.; Wang, J. W. Synthesis, characterization, photocleavage, cytotoxicity *in vitro*, apoptosis, and cell cycle arrest of ruthenium(II) complexes. *J. Coord. Chem.* **2012**, *65*, 1781–1791.
52. Patel, M. N.; Gandhi, D. S.; Parmar, P. A.; Joshi, H. N. DNA-binding and cleavage activity of polypyridyl ruthenium(II) complexes. *J. Coord. Chem.* **2012**, *65*, 1926–1936.
53. Liu, X. W.; Chen, Y. D.; Li, L. Synthesis, DNA-binding, and photocleavage properties of Ru(II) complexes containing dppz-based ligand. *J. Coord. Chem.* **2012**, *65*, 3050–3063.